Robotica (2016) volume 34, pp. 2116–2139. © Cambridge University Press 2015
doi:10.1017/S0263574715000247

Time-optimal path tracking for robots under dynamics constraints based on convex optimization

Qiang Zhang†‡, Shurong Li‡, Jian-Xin Guo† and Xiao-Shan Gao† *

†*Academy of Mathematics and Systems Science, Chinese Academy of Sciences, Beijing, China*
‡*Department of Automation, China University of Petroleum (East China), Qingdao, China*

(Accepted March 2, 2015. First published online: April 15, 2015)

SUMMARY
To fully utilize the dynamic performance of robotic manipulators and enforce minimum motion time in path tracking, the problem of minimum time path tracking for robotic manipulators under confined torque, change rate of the torque, and voltage of the DC motor is considered. The main contribution is the introduction of the concepts of virtual change rate of the torque and the virtual voltage, which are linear functions in the state and control variables and are shown to be very tight approximation to the real ones. As a result, the computationally challenging non-convex minimum time path tracking problem is reduced to a convex optimization problem which can be solved efficiently. It is also shown that introducing dynamics constraints can significantly improve the motion precision without costing much in motion time, especially in the case of high speed motion. Extensive simulations are presented to demonstrate the effectiveness of the proposed approach.

KEYWORDS: Robotic manipulators; Motor dynamics; Path tracking; Optimal trajectory; Optimal control; Convex optimization.

1. Introduction

For the purpose of maximizing productivity, the problem of minimum time path tracking of robotic manipulators is widely studied. Basically, two kinds of constraints are considered in the minimum time path tracking problem. Kinematics (velocity, acceleration, jerk, and jounce) constrained minimum time trajectory planning problems were studied in refs. [1]–[7]. On the other hand, dynamics (torque, change rate of the torque, and drive dynamics) constrained minimum time trajectory planning problems were studied in refs. [8]–[13]. In this paper, we will adopt the dynamics constrained approach due to its ability to more accurately describe the dynamic power of the robotic manipulators.

As a basic problem in the motion planning, the torque constrained minimum time trajectory planning has been intensively studied and there already exist several efficient algorithms. Bobrow *et al.*[8] and Sadigh and Mansouri[13] applied phase plane analysis approaches to solve the problem. Chen and Desrochers[14] used the Pontryagin maximum principle and the shooting algorithm. Korayem *et al.* used the dynamic programming approach.[11] Recently, Verscheure *et al.*[10] made a significant contribution by parameterizing this optimal control problem into a convex optimization problem. This direct transcription method has the advantage that solutions can be found efficiently for any complicated tool-pathes and robotic structures. Reynoso-Mora *et al.* considered a more general model for the torque and reduced the path tracking problem to a convex optimization problem.[15] In ref. [16], a linear program based method is proposed to solve this problem.

It is well-known that the torque functions obtained under confined torques are usually discontinuous, which are physically unrealistic and may cause significant tracking errors in high speed motions.[10,14] Therefore, as a problem for further study, Verscheure *et al.*[10] suggested that "the application of the presented method to sequential convex approximations of problems which take

* Corresponding author. E-mail: xgao@mmrc.iss.ac.cn

https://doi.org/10.1017/S0263574715000247 Published online by Cambridge University Press

into account constraints on the change rate of the torque will be investigated." The main difficulty in solving this problem is that it limits on the change rate of the torque that will lead to a non-convex optimization problem. This problem is partially solved by Ardeshiri *et al.*,[19] who only considered the counter-electromotive force and obtained a convex problem. In ref. [20], the minimum time path tracking problem under the confined change rate of the torque was reduced approximately into a convex optimization problem. In a recent and independent study,[21] Debrouwere *et al.* proposed an efficient sequential convex programming approach to solve the problem by writing the non-convex constraints as a difference of convex functions.

Besides the torque, the drive dynamic quantities such as the voltage of the DC motor constitute an important part of the complete robot dynamics, especially in the cases of high velocity movement and high varying loads.[17] To achieve minimum motion time, the velocity of each manipulator joint can be very high. So including the drive dynamics in the minimum time trajectory planning is necessary. Ardeshiri *et al.*[19] considered a simplified motor dynamics and studied a speed dependent torque constrained minimum time trajectory planning problem. Tarkiainen and Shiller[18] ignored manipulator gravity and studied the rigid manipulator dynamics and motor dynamics governed minimum time trajectory planning problem.

In this paper, it is shown that the problem of minimum time path tracking for robots under confined torque, change rate of the torque, and the voltage can be solved efficiently with convex optimization algorithms. To compute the optimum trajectory efficiently, the concepts of virtual change rate of the torque and the virtual voltage are introduced, which are linear functions in the state and control variables and are very tight approximation to the real change rate of the torque and the voltage. Technically, we use a novel linearization technique based on solutions of the easier minimum time path tracking problem under confined torque only. As a result, the minimum time path tracking problem under virtual change rate of the torque and the virtual voltage can be parameterized into a convex optimization problem which can be solved efficiently. It is also shown that when these virtual quantities are bounded, the real corresponding quantities are also bounded, which guaranties the feasibility of the solution.

According to the simulation results, the proposed approach has the following advantages. Firstly, by adding the change rate of the torque constraint and the voltage constraint, the tracking error can be reduced significantly (for example 90% in our example) with the cost of a very small increase (7% in our example) of tracking time, especially in high speed motions. Secondly, the newly introduced convex problem is a very nice approximation to the original problem. According to our experiments, the difference of the optimum solutions for the two problems is very small. Thirdly, in terms of computational efficiency, the original problem is unsolvable for modest sized discretization, while the new one can be solved within seconds and thus can be used in practice.

Different from the works of Ardeshiri *et al.*[19] and Debrouwere *et al.*[21] who simplified the motor dynamics and Tarkiainen and Shiller[18] who neglected the manipulator gravity, the proposed approach considers the complete robot dynamics, including the motor dynamics with counter-electromotive force and induced electromotive force, and rigid dynamics with manipulator gravity. It is shown that the three constraints considered in this paper give an appropriate description to the dynamic ability of the robotic manipulators. Comparing to ref. [20], the more difficult constraint of motor voltage is considered. Comparing to ref. [21], our method need to solve two convex optimization problems whose constraints are linear, while a series of convex optimization problems need to be solved in ref. [21]. Also, the SCP method proposed in ref. [21] cannot be used to solve the problem in this paper.

The rest of the paper is organized as follows. In Section 2, the rigid manipulator dynamics and motor dynamics are stated and the dynamic constraints are presented. In Section 3, a convex optimal control formulation is given for the desired trajectory planning problem and feasibility analysis is discussed. The details of the numerical solution are presented in Section 4. Numerical examples are given in Section 5. Conclusions are given in Section 6.

2. System Dynamics Description

In this section, constraints for the rigid robotic manipulator dynamics and the armature-controlled DC motor dynamics are used to achieve a more complete description of the robot dynamic ability.

https://doi.org/10.1017/S0263574715000247 Published online by Cambridge University Press

2.1. Dynamics of rigid robotic manipulators

The dynamic model of an n-DOF robotic manipulator is assumed to satisfy the following equation:[9]

$$\tau = \mathbf{M}(\mathbf{q})\ddot{\mathbf{q}} + \dot{\mathbf{q}}^{\mathrm{T}}\mathbf{C}(\mathbf{q})\dot{\mathbf{q}} + \mathbf{G}(\mathbf{q}), \tag{1}$$

where $\tau = (\tau_1, \ldots, \tau_n)^{\mathrm{T}} \in \mathbf{R}^n$ is the vector of actuator torques, $\mathbf{q} \in \mathbf{R}^n$ is the vector of joint angular positions and $\dot{\mathbf{q}} = \frac{\mathrm{d}\mathbf{q}}{\mathrm{dt}}, \ddot{\mathbf{q}} = \frac{\mathrm{d}\dot{\mathbf{q}}}{\mathrm{dt}}, \mathbf{M}(\mathbf{q}) \in \mathbf{R}^{n\times n}$ is the inertia matrix of the manipulator, $\mathbf{C}(\mathbf{q}) \in (\mathbf{R}^n)^{n\times n}$ is a matrix, whose elements are in $\mathbf{R}^n$, representing the coefficients of the centrifugal and Coriolis forces, and $\mathbf{G}(\mathbf{q}) \in \mathbf{R}^n$ is the vector of gravitational torque. For simplicity, viscous, and static friction terms have been neglected in the dynamic model. The angular position $\mathbf{q}$ is assumed to be a function in a parameter $s \in [0, 1]$. The aim of trajectory planning is to compute the *parameter velocity* $\dot{s} = \frac{\mathrm{ds}}{\mathrm{dt}}$.

Denote $' = \frac{\mathrm{d}}{\mathrm{ds}}$ and $\cdot = \frac{\mathrm{d}}{\mathrm{dt}}$. The joint kinematics can be formulated as follows:

Joint velocity: $\dot{\mathbf{q}}(t) = \mathbf{q}'(s(t))\,\dot{s}(t)$,

Joint acceleration: $\ddot{\mathbf{q}}(t) = \mathbf{q}'(s(t))\,\ddot{s}(t) + \mathbf{q}''(s(t))\,\dot{s}^2(t)$.

Using these kinematic equations, the dynamic model (1) of the robotic manipulator can be written as a function in the path parameter s

$$\tau = \mathbf{m}(s)\,\ddot{s} + \mathbf{c}(s)\,\dot{s}^2 + \mathbf{g}(s), \tag{2}$$

where

$$\begin{aligned}
\mathbf{m}(s) &= \mathbf{M}(\mathbf{q}(s))\,\mathbf{q}'(s) \in \mathbf{R}^n,\\
\mathbf{c}(s) &= \mathbf{M}(\mathbf{q}(s))\,\mathbf{q}''(s) + \mathbf{q}'(s)^{\mathrm{T}}\mathbf{C}(\mathbf{q}(s))\,\mathbf{q}'(s) \in \mathbf{R}^n,\\
\mathbf{g}(s) &= \mathbf{G}(\mathbf{q}(s)) \in \mathbf{R}^n.
\end{aligned}$$

2.2. Motor dynamics

DC motors are used to drive the manipulator joints. To describe the dynamics of the ith motor, we need the following physical parameters: the resistance of armature circuit (R_i), the inductance of armature circuit (L_i), the voltage constant of the motor ($K_i{}^e$), the gear ratio (N_i), the torque constant ($K_i{}^\tau$), and the control voltage (u_i) of the ith motor. Then, the actuator dynamic of the ith joint is described as[17]

$$\begin{aligned}
u_i &= L_i\dot{I}_i + R_i I_i + K_i{}^e\dot{\theta}_i, \quad i = 1, 2, \ldots, n,\\
\dot{\theta}_i &= N_i\dot{q}_i, \quad i = 1, 2, \ldots, n,
\end{aligned}$$

where I_i is the armature current and θ_i is the angular position of the ith rotor. The output torque of the ith DC motor is proportional to the motor current

$$\tau_i = N_i K_i{}^\tau I_i. \tag{3}$$

Then the actuator dynamics can be rewritten as the following vector form:

$$\mathbf{u} = \mathbf{L}\dot{\tau} + \mathbf{D}\tau + \mathbf{K}\dot{s}, \tag{4}$$

where

$$\begin{aligned}
\mathbf{L} &= \mathrm{diag}\left\{\tfrac{L_i}{N_i K_i{}^\tau},\ i = 1, 2, \ldots, n\right\} \in \mathbf{R}^{n\times n},\\
\mathbf{D} &= \mathrm{diag}\left\{\tfrac{R_i}{N_i K_i{}^\tau},\ i = 1, 2, \ldots, n\right\} \in \mathbf{R}^{n\times n},\\
\mathbf{K}_c &= \mathrm{diag}\{K_i{}^e N_i,\ i = 1, 2, \ldots, n\} \in \mathbf{R}^{n\times n},
\end{aligned}$$

are diagonal positive definite matrixes and $\mathbf{K} = \mathbf{K_c}\mathbf{q}' \in \mathbf{R}^n$. For convenience, we use $\mathbf{L}_{ii}$, $\mathbf{D}_{ii}$, and $\mathbf{K_c}_{ii}$ to denote $\mathbf{L}(i, i)$, $\mathbf{D}(i, i)$, and $\mathbf{K_c}(i, i)$, respectively.

https://doi.org/10.1017/S0263574715000247 Published online by Cambridge University Press

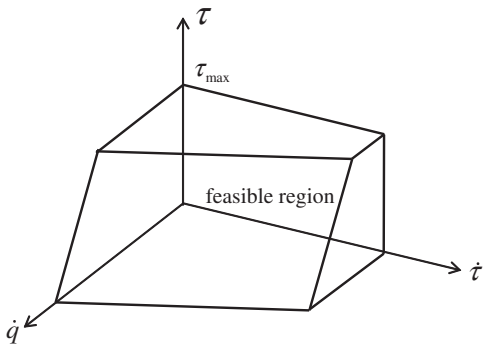


Fig 1. Feasible region for an electrical brushless DC-motor.

2.3. Dynamics constraints

In this section, the constraints adopted in this paper will be given.

2.3.1. Torque constraints. The heat production of the ith motor can be calculated by $Q_i = {I_i}^2 R_i$. Considering the thermal dissipation capacity of the motor, the armature current should be limited. Due to Eq. (3), the torques clearly have the following constraints:

$$-\tau_{\mathrm{B}} \leq \tau \leq \tau_{\mathrm{B}}, \tag{5}$$

where $\tau_{\mathrm{B}} = [\tau_{1,B}, \ldots, \tau_{n,B}]$ and $\tau_{i,B} = N_i {K_i}^{\tau} I_{i,B}$. $I_{i,B}$ is the current bound of the ith motor.

2.3.2. Constraints on the change rate of the torque. As pointed in ref. [10], the limited bandwidth of the physical actuator implies that infinitely fast torque jumps cannot be realized and therefore, constraints on the change rate of the torque need to be added

$$-\dot{\tau}_{\mathrm{B}} \leq \dot{\tau} \leq \dot{\tau}_{\mathrm{B}}, \tag{6}$$

where $\dot{\tau}_{\mathrm{B}}$ is the bound vector for the change rate of the torque.

2.3.3. Voltage constraints. The dynamic performance of the whole system is limited by the torque constraint at low rotating speed because of the heat produced in the motor. When the rotating speed increases or the torque has fast changes, the motor voltage would be saturated and the maximum torque of the motor may not be maintained at the bound. In this case, the dynamic performance of the system is charged by the DC-voltage constraints, written as

$$-\mathbf{u}_{\mathrm{B}} \leq \mathbf{u} \leq \mathbf{u}_{\mathrm{B}}, \tag{7}$$

where $\mathbf{u}_{\mathrm{B}}$ is the bound vector for the voltage.

The feasible region described by the three constraints in the $\dot{q}$-$\dot{\tau}$-τ space for the DC-motor is shown in Fig. 1.

The commonly considered dynamic constraints in the trajectory planning problems are only torque constraints, which have several excellent computation properties, such as convex structure, unique optimal solution, efficient numerical solution algorithms.[1,8,10,14] But there also exist drawbacks in this strategy. The maximum joint torque decreases along with increased joint speed and fast changed torque, as shown in Fig. 2. So the setting of the torque limits should consider not only the heat production but also the effectiveness of the maximum torques affected by joint speed, change ratio of the torque, and the voltage constraint. As a consequence, when using velocity constraints $|\dot{\mathbf{q}}| \leq \dot{\mathbf{q}}_B$, conservative torque bounds must be used, which is the cube shown in Fig. 2.

From Fig. 2, it is obvious that incorporating manipulator dynamics and motor dynamics can solve the problem. But the planning problem under motor dynamics constraints is not studied thoroughly, because introducing the motor dynamics makes the trajectory planning problem non-convex and numerical solving challenging.

https://doi.org/10.1017/S0263574715000247 Published online by Cambridge University Press

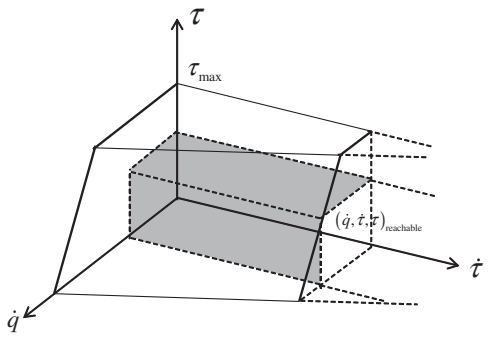


Fig 2. Feasible region for confined $\tau,\ \dot{q},\ \dot{\tau}$.

3. Time Optimal Trajectory Planning with Confined Dynamics Constraints

In this section, it is shown that the optimal trajectory planning problem under dynamic constraints can be reduced to a convex optimization problem by introducing the concepts of virtual voltage and virtual change rate of the torque.

3.1. Problem statement as an optimal control problem

In this section, the time optimal trajectory planning problem considered in this paper will be presented.

In task space, a parametric path is given

$$\mathbf{r}(s) = [y_1(s), \ldots, y_n(s)]^{\mathrm{T}}, \quad s \in [0, 1], \tag{8}$$

which will be traversed by the end effector of the robot. The corresponding joint path $\mathbf{q}(s)$ in the joint space is also assumed to be determined by considering task requirements, obstacle avoidance, singularity avoidance, etc. Hence, a certain kinematics map between $\mathbf{r}(s)$ and $\mathbf{q}(s)$ exists.

Similar to ref. [22] , the following assumptions are applied in this paper. The path $\mathbf{q}(s)$ is assumed to have bounded and uniformly continuous derivatives up to the third order. The robot manipulator is operated away from any singularity. Furthermore, $\dot{s} > 0$ for $s \in (0, 1)$ is assumed, meaning that the robot does not stop during the traversal. With this assumption, $\dot{s}$ is treated as a function in s in the rest of the paper.

It is assumed that the time optimal trajectory is governed by the manipulator dynamics (2) and the motor dynamics (4), simultaneously. Let

$$x_1(s) = \dot{s}^2(s), \quad x_2(s) = \ddot{s}(s), \quad s \in [0, 1]. \tag{9}$$

From Eq. (2), the joint torque can be formulated as a linear function in x_1 and x_2

$$\tau = \mathbf{m}(s)\, x_2 + \mathbf{c}(s)\, x_1 + \mathbf{g}(s). \tag{10}$$

We introduce the following new variable to cover the motor dynamics:

$$x_3(s) = \frac{\dddot{s}(s)}{\dot{s}(s)}, \quad s \in [0, 1]. \tag{11}$$

The change rate vector of joint torques can be formulated as

$$\dot{\tau} = \tau' \dot{s} = \tau' \sqrt{x_1} = \mathbf{m}\, \ddot{s} + \left(\mathbf{m}' + 2\mathbf{c}\right) \dot{s} \ddot{s} + \mathbf{c}' \dot{s}^3 + \mathbf{g}' \dot{s} \tag{12}$$

https://doi.org/10.1017/S0263574715000247 Published online by Cambridge University Press

where

$$\begin{aligned}\tau' &= \mathbf{m}x_3 + (\mathbf{m}' + 2\mathbf{c})x_2 + \mathbf{c}'x_1 + \mathbf{g}'\\ \mathbf{m}'(s) &= \mathbf{M}'\mathbf{q}' + \mathbf{M}\mathbf{q}'',\\ \mathbf{c}'(s) &= \mathbf{M}'\mathbf{q}'' + \mathbf{M}\mathbf{q}''' + \mathbf{q}'^{\mathrm{T}}\mathbf{C}'\mathbf{q}' + \mathbf{q}''^{\mathrm{T}}\mathbf{C}\mathbf{q}' + \mathbf{q}'^{\mathrm{T}}\mathbf{C}\mathbf{q}'',\\ \mathbf{g}'(s) &= \mathbf{G}'.\end{aligned}$$

The motor dynamics (4) can be written as

$$\mathbf{u} = \mathbf{L}\dot{\tau} + \mathbf{D}\tau + \mathbf{K}\dot{s} = \left(\mathbf{L}\tau' + \mathbf{K}\right)\sqrt{x_1} + \mathbf{D}\tau. \tag{13}$$

The state vector (x_1, x_2, x_3) satisfies the following relations:

$$\frac{\mathrm{d}x_1}{\mathrm{d}s} = 2x_2, \quad \frac{\mathrm{d}x_2}{\mathrm{d}s} = x_3. \tag{14}$$

The following boundary conditions of joint velocities and joint torques are assumed:

$$\begin{aligned}&\dot{\mathbf{q}}(0) = \mathbf{q}'(0)\sqrt{x_1(0)} = \dot{\mathbf{q}}_0,\\ &\dot{\mathbf{q}}(1) = \mathbf{q}'(1)\sqrt{x_1(1)} = \dot{\mathbf{q}}_{\mathrm{f}},\\ &\tau(0) = \mathbf{m}(0)x_2(0) + \mathbf{c}(0)x_1(0) + \mathbf{g}(0) = 0,\\ &\tau(1) = \mathbf{m}(1)x_2(1) + \mathbf{c}(1)x_1(1) + \mathbf{g}(1) = 0.\end{aligned} \tag{15}$$

In order to obtain $x_1(0)$, $x_1(1)$, $x_2(0)$, $x_2(1)$, we assume that $\mathbf{q}(0)'$, $\mathbf{q}(1)'$, $\mathbf{m}(0)$, $\mathbf{m}(1)$ are not the zero vector.

Finally, the path following minimum time trajectory planning problem can be described as the following nonlinear optimal control problem:

$$\begin{aligned}&\min_{x_3} \quad J_{\mathrm{obj}} = \int_0^1 \frac{1}{\sqrt{x_1}}\mathrm{d}s\\ &\text{s.t. } x_1'(s) = 2x_2, \quad x_2'(s) = x_3, \quad s \in [0, 1]\\ &\quad x_1(s) > 0, \quad s \in (0, 1),\\ &\quad -\tau_{\mathrm{B}} \le \tau(s) \le \tau_{\mathrm{B}},\\ &\quad -\dot{\tau}_{\mathrm{B}} \le \dot{\tau}(s) \le \dot{\tau}_{\mathrm{B}},\\ &\quad -\mathbf{u}_{\mathrm{B}} \le \mathbf{u}(s) \le \mathbf{u}_{\mathrm{B}},\end{aligned} \tag{16}$$

where $\tau(s)$, $\tau'(s)$, $\dot{\tau}(s)$, and $\mathbf{u}(s)$ are defined in Eqs. (10), (12) and (13), and the initial values $x_1(0)$, $x_1(1)$, $x_2(0)$, $x_2(1)$ are obtained from Eq. (15).

Problem (16) is governed by a system of second order equations. The robotic rigid dynamics act as process state constraint and the motor dynamics act as the process state-control constraint. Because of the non-convexity of the dynamic constraints, problem (16) is non-convex and numerical solution for such a problem is generally very difficult to compute.[10]

3.2. Problem reduction to a convex optimal control problem

In this section, we will show that problem (16) can be reduced to a convex optimization problem under certain conditions.

To make the reduction, first consider the following simpler optimization problem by dropping the voltage and the change rate of the torque constraints from Eq. (16)

$$\begin{aligned}&\min_{x_2} \quad \int_0^1 \frac{1}{\sqrt{x_1}}\mathrm{d}s\\ &\text{s.t. } x_1'(s) = 2x_2, \quad x_1(0) = x_{1,0}, \quad x_1(1) = x_{1,1},\\ &\quad -\tau_{\mathrm{B}} \le \tau(s) \le \tau_{\mathrm{B}}.\end{aligned} \tag{17}$$

From the proof of Theorem 2 in Bobrow *et al.*[8] problem (17) has the following useful property.

https://doi.org/10.1017/S0263574715000247 Published online by Cambridge University Press

THEOREM 1. *The optimal solution* $\dot{s}_\tau(s)$ *to problem (17) is unique and maximum for any* $s \in [0, 1]$. *That is, let* $\dot{s}(s)$ *be any other parameter velocity satisfying the constraints of Eq. (17). Then,* $0 \le \dot{s}(s) \le \dot{s}_\tau(s)$ *for all* $s \in [0, 1]$.

According to the formulation of problem (16), it is easy to see that the optimal parameter velocity of problem (16), denoted by $\dot{s}_\delta(s)$, also satisfies the constraints of problem (17). By Theorem 1, we have $\dot{s}_\delta(s) \le \dot{s}_\tau(s)$ for all $s \in [0, 1]$.

If the voltage bound and the bound for the change rate of the torque are set to approach infinite, then it is expected that problem (16) will degenerate to problem (17) and the corresponding optimal state satisfies

$$(\dot{s}_\tau(s) - \dot{s}_\delta(s)) \to 0^+, \quad s \in [0, 1].$$

On the contrary, if the bounds $\mathbf{u}_B$ and $\dot{\tau}_\mathrm{B}$ are set to be small enough, then the movement would be completely charged by the voltage or the change rate of the torque constraints and $\dot{s}_\delta(s)$ will be strictly smaller than $\dot{s}_\tau(s)$. So for appropriately chosen voltage and torque change rate bounds, we have reason to believe that the optimal parameter velocity $\dot{s}_\delta(s)$ of problem (16) only have little deviation from the typical $\dot{s}_\tau(s)$, and this fact can be used to simplify problem (16). The examples in the Section 5 can also support this assertion.

In what below, we will show how to change the two nonlinear constraints $-\dot{\tau}_\mathrm{B} \le \dot{\tau} \le \dot{\tau}_\mathrm{B}$ and $-\mathbf{u}_\mathrm{B} \le \mathbf{u} \le \mathbf{u}_\mathrm{B}$ into linear ones. The commonly used method to linearize a nonlinear function is based on Taylor expansion. Since the Taylor expansion only gives good approximation locally, the corresponding nonlinear optimization solution is usually an iteratively solving process. Here we propose a novel linearization strategy for our nonlinear constraints, where the nonlinear constraints are nicely and globally approximated by linear functions.

Let $\dot{s}_\tau(s)$ be the unique optimal solution to problem (17). Define the following *virtual change rate of the torque* with the help of $\dot{s}_\tau(s)$:

$$\tilde{\dot{\tau}}(s) = \tau'(s)\dot{s}_\tau(s) = (\mathbf{m}x_3 + \left(\mathbf{m}' + 2\mathbf{c}\right)x_2 + \mathbf{c}'x_1 + \mathbf{g}')\dot{s}_\tau(s), \tag{18}$$

which is a linear function in (x_1, x_2, x_3). Due to Theorem 1, $\left|\tilde{\dot{\tau}}_i(s)\right| \ge |\dot{\tau}_i(s)|$ holds $s \in [0, 1]$ and $i = 1, 2, \ldots, n$. So the new constraint $-\dot{\tau}_\mathrm{B} \le \tilde{\dot{\tau}} \le \dot{\tau}_\mathrm{B}$ implies the original constraint $-\dot{\tau}_\mathrm{B} \le \dot{\tau} \le \dot{\tau}_\mathrm{B}$. Furthermore, it will be shown in Section 5 that the virtual change rate of the torque gives a very good approximation to the real change rate of the torque. So, we can replace the constraint $-\dot{\tau}_\mathrm{B} \le \dot{\tau} \le \dot{\tau}_\mathrm{B}$ by $-\dot{\tau}_\mathrm{B} \le \tilde{\dot{\tau}} \le \dot{\tau}_\mathrm{B}$ in problem (16).

For the voltage, define the following *virtual voltage* of the DC motor with the help of $\dot{s}_\tau(s)$:

$$\tilde{\mathbf{u}} = (\mathbf{L}\tau' + \mathbf{K})\dot{s}_\tau + \mathbf{D}\tau, \tag{19}$$

which is a linear function in (x_1, x_2, x_3). Note that $\tilde{\dot{\tau}}(s)$ and $\tilde{\mathbf{u}}(s)$ defined in Eq. (18) are linear in x_1, x_2, x_3. Also note that $\dot{s}(s)$ is approximated by $s_\tau(s)$ instead of the maximal value of $\dot{s}(s)$. This makes $\tilde{\dot{\tau}}(s)$ and $\tilde{\mathbf{u}}(s)$ to be nice approximations of $\dot{\tau}(s)$ and $\mathbf{u}(s)$, respectively.

Using the virtual change rate of the torque and the virtual voltage to approximate the real change rate of the torque and the real voltage, the problem can be reduced to the following optimal control problem:

$$\begin{aligned} &\min_{x_3} \quad J_\mathrm{obj} = \int_0^1 \tfrac{1}{\sqrt{x_1}}\mathrm{d}s \\ \text{s.t. } &x_1'(s) = 2x_2, \quad x_2'(s) = x_3, \quad s \in [0, 1], \\ &x_1(s) > 0, \quad s \in (0, 1), \\ &-\tau_\mathrm{B} \le \tau(s) \le \tau_\mathrm{B}, \\ &-\dot{\tau}_\mathrm{B} \le \tilde{\dot{\tau}}(s) \le \dot{\tau}_\mathrm{B}, \\ &-\mathbf{u}_\mathrm{B} \le \tilde{\mathbf{u}}(s) \le \mathbf{u}_\mathrm{B}, \end{aligned} \tag{20}$$

where $\tilde{\dot{\tau}}(s)$ and $\tilde{\mathbf{u}}(s)$ are defined in Eqs. (18) and (19), respectively.

Since the constraints of problem (20) are linear and its objective function is convex,[10] problem (20) is convex.

https://doi.org/10.1017/S0263574715000247 Published online by Cambridge University Press

3.3. Feasibility analysis of the reduced problem

In this section, a condition is given under which a solution to problem (20) is also a feasible to problem (16), meaning that the constraints of problem (16) are satisfied.

As mentioned in the preceding section, the constraint about the virtual change rate of the torque implies the constraint on the real change rate of the torque. For the virtual voltage, we assume that the dynamic parameters satisfy the following conditions:

$$\begin{cases} u_{i,\mathrm{B}} - \mathbf{D}_{ii}\tau_i \geq 0, \\ -u_{i,\mathrm{B}} - \mathbf{D}_{ii}\tau_i \leq 0, \end{cases} \quad \text{for all} \quad \tau_i \in [-\tau_{i,B}, \quad \tau_{i,B}], \quad i = 1, 2, \ldots, n. \tag{21}$$

The following theorem shows that the above conditions are sufficient for the solutions of problem (20) to be feasible.

THEOREM 2. *Suppose that condition* (21) *is valid and* x_1^*, x_2^*, x_3^* *are optimal solutions to problem* (20). *Then* x_1^*, x_2^*, x_3^* *are feasible to problem* (16). *More precisely, let*

$$\tilde{\mathbf{u}}^* = (\mathbf{L}\tau'^* + \mathbf{K})\dot{s}_\tau + \mathbf{D}\tau^*.$$

be the optimal virtual voltage for problem (20) *and*

$$\mathbf{u}^* = \left(\mathbf{L}\tau'^* + \mathbf{K}\right)\sqrt{x_1^*} + \mathbf{D}\tau^*.$$

Then $-\mathbf{u}_B \leq \mathbf{u}^*(s) \leq \mathbf{u}_B$ *for all* $s \in [0, 1]$.

Proof. We prove the theorem by reduction ad absurdum. Take the ith joint for example and use u_i^* to represent the ith component of $\mathbf{u}^*$. Assume u_i^* is not feasible for problem (16) in certain parameter interval $[s_a, s_b] \subset [0, 1]$ meaning

I. $u_i^*(s) > u_{i,B}$

or

II. $u_i^*(s) < -u_{i,B}$

for $s \in [s_a, s_b]$.

We will prove cases I and II are not possible.

Case I. We first show that $\dot{s}_\tau(s) = \sqrt{x_1^*(s)}$ is impossible for any $s \in [s_a, s_b]$. Indeed, $\dot{s}_\tau(s) = \sqrt{x_1^*(s)}$ implies $\tilde{u}_i^*(s) = u_i^*(s) > u_{i,B}$, a contradiction. Since $\tilde{\mathbf{u}}^*(s)$ satisfies the constraints of Eq. (17), we have $\dot{s}_\tau(s) > \sqrt{x_1^*(s)}$ for $s \in [s_a, s_b]$. For $s \in [s_a, s_b]$, from $u_i^*(s) > u_{i,B}$ and Eq. (21), we have

$$\left(\mathbf{L}_{ii}\tau_i'^* + \mathbf{K}_i\right)\sqrt{x_1^*} = u_i^*(s) - \mathbf{D}_{ii}\tau_i^* > u_{i,\mathrm{B}} - \mathbf{D}_{ii}\tau_i^* \geq 0,$$

which means $\left(\mathbf{L}_{ii}\tau_i'^* + \mathbf{K}_i\right) > 0$. So for an $s \in [s_a, s_b]$, since $\dot{s}_\tau(s) > \sqrt{x_1^*(s)}$, we have

$$\tilde{u}_i^*(s) - \mathbf{D}_{ii}\tau_i^* = \left(\mathbf{L}_{ii}\tau_i'^* + \mathbf{K}_i\right)\dot{s}_\tau > \left(\mathbf{L}_{ii}\tau_i'^* + \mathbf{K}_i\right)\sqrt{x_1^*} = u_i^*(s) - \mathbf{D}_{ii}\tau_i^*$$

or $\tilde{u}_i^*(s) > u_i^*(s) \geq u_{i,B}$. This is contradictory with $-u_{i,B} \leq \tilde{u}_i^*(s) \leq u_{i,B}$, so this case is not possible.

Case II. Similarly as case I. Here $u_i^*(s) < -u_{i,B}$, hence

$$\left(\mathbf{L}_{ii}\tau_i'^* + \mathbf{K}_i\right)\sqrt{x_1^*} = u_i^* - \mathbf{D}_{ii}\tau_i^* < -u_{i,\mathrm{B}} - \mathbf{D}_{ii}\tau_i^* \leq 0,$$

meaning $(\mathbf{L}_{ii}\tau_i'^* + \mathbf{K}_i) < 0$. So at certain parametric value, $\tilde{u}_i^* < u_i^* \leq -u_{i,B}$ and a contradiction is obtained. The theorem is proved.

4. Numerical Solution

The time minimum trajectory with rigid manipulator dynamics and motor dynamics constraints can be obtained by executing the following three steps:

https://doi.org/10.1017/S0263574715000247 Published online by Cambridge University Press

1. Compute the unique maximum velocity trajectory $\dot{s}_\tau(s)$ by solving the torque constrained minimum time motion problem using existing efficient methods, such as Verscheure *et al.*,[10] Fan *et al.*,[24] Zhang *et al.*,[25] or Yuan *et al.*[26]

2. Use the parametric velocity $\dot{s}_\tau(s)$ obtained in the first step to construct the virtual change rate of the torque $\tilde{\dot{\tau}}$ in Eq. (18) and the virtual voltage function $\tilde{\mathbf{u}}$ in Eq. (19) and then a gradient based direct transcription method is used to compute the optimal solution $\dot{s}_v(s)$ of the convex problem (20) efficiently, which will be discussed in this section.

3. The solution $\dot{s}_v(s)$ obtained in step 2 is a very tight approximation to the optimal solution of the original problem (16). Therefore, $\dot{s}_v(s)$ can be used as the initial value to solve problem (16) using similar procedures for solving problem (20), which is generally convergent. On the other hand, with a rough guess as the initial value, numerical solution to problem (16) fails in most of the cases.

4.1. Trajectory parameterization

Typical direct transcription methods are realized by reformulating the optimal control problem as a large sparse optimization problem. To this end, the trajectory parameterization is needed.

As mentioned in ref. [20], a B-spline curve of degree p is applied to parameterize the time varying trajectory $x_1(s)$. According to the property of B-splines,[29] in order for the boundary values $x_1(0)$ and $x_1(1)$ to be fixed, the sequence of grid nodes must be written as

$$\mathbf{s_n} = \left[\underbrace{0, \ldots, 0}_{p+1}, s_1, \ \ldots, \ s_i, \ \ldots, \quad s_{K-p+1}, \ \underbrace{1, \ldots, 1}_{p+1}\right], \tag{22}$$

where K is a positive integer.

Since the torque and joint voltage are bounded, the third order derivative information of the parameter with respect to time should exist. So let $p = 2$ meaning that the 3-order B-spline is suitable for our problem. Then the state $x_1(s)$ of problem (20) can be approximated by the following B-spline curve in the parameter interval [0, 1].

$$x_1(s) \approx \tilde{x}_1(s) = \sum_{i=0}^{K+1} N_{i,p}(s)\hat{a}_i, \tag{23}$$

where $\hat{a}_i$ is the parameter value at the ith grid, and $N_{i,p}(s)$ denotes the ith basis function defined as

$$N_{i,0}(s) = \begin{cases} 1 & \text{if } \mathbf{s_n}(i) \le s \le \mathbf{s_n}(i+1) \\ 0 & \text{otherwise} \end{cases}, \quad i = 0, \ldots, K+p+1,$$

$$N_{i,p}(s) = \frac{s - \mathbf{s_n}(i)}{\mathbf{s_n}(i+p) - \mathbf{s_n}(i)} N_{i,p-1}(s) + \frac{\mathbf{s_n}(i+p+1) - s}{\mathbf{s_n}(i+p+1) - \mathbf{s_n}(i+1)} N_{i+1,p-1}(s), \, i = 0, \ldots, K+1.$$

According to the properties of B-splines, the derivative information of the trajectory $x_1(s)$ w.r.t s can be obtained by

$$x_2(s) = \frac{1}{2} x_1{}'(s) = \frac{1}{2}\frac{\mathrm{d}x_1(s)}{\mathrm{d}s} = \frac{1}{2}\sum_{i=0}^{K+1} N_{i,p}^{'}(s)\hat{a}_i, \tag{24}$$

$$x_3(s) = x_2{}'(s) = \frac{\mathrm{d}x_2(s)}{\mathrm{d}s} = \frac{1}{2}\sum_{i=0}^{K+1} N_{i,p}^{''}(s)\hat{a}_i, \tag{25}$$

https://doi.org/10.1017/S0263574715000247 Published online by Cambridge University Press

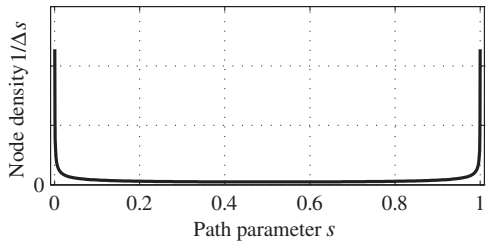


Fig 3. Allocated grid node density.

where

$$N_{i,p}^{'}(s)=\frac{p}{\mathbf{s_n}(i+p)-\mathbf{s_n}(i)}N_{i,p-1}(s)-\frac{p}{\mathbf{s_n}(i+p+1)-\mathbf{s_n}(i+1)}N_{i+1,p-1}(s),$$
$$N_{i,p}^{''}(s)=\frac{p}{\mathbf{s_n}(i+p)-\mathbf{s_n}(i)}N^{'}{}_{i,p-1}(s)-\frac{p}{\mathbf{s_n}(i+p+1)-\mathbf{s_n}(i+1)}N^{'}{}_{i+1,p-1}(s),$$

with $N_{i,p-1}^{'}(s)=\frac{\mathrm{d}}{\mathrm{d}s}N_{i,p-1}(s)=\frac{p-1}{\mathbf{s_n}(i+p-1)-\mathbf{s_n}(i)}N_{i,p-2}(s)-\frac{p-1}{\mathbf{s_n}(i+p)-\mathbf{s_n}(i+1)}N_{i+1,p-2}(s)$,
$N_{i+1,p-1}^{'}(s)=\frac{\mathrm{d}}{\mathrm{d}s}N_{i+1,p-1}(s)=\frac{p-1}{\mathbf{s_n}(i+p)-\mathbf{s_n}(i+1)}N_{i+1,p-2}(s)-\frac{p-1}{\mathbf{s_n}(i+p+1)-\mathbf{s_n}(i+2)}N_{i+2,p-2}(s)$.

4.2. Spline nodes allocation

Usually the nodes sequence of Eq. (22) is assumed to be uniformly distributed in the parameter domain. Here based on sensitivity analysis, we apply a non-uniform distribution to allocate the node sequence.

The gradient of the objective function of problem (20) with respect to the spline parameter $\hat{a}_i$ can be calculated by

$$\begin{aligned}\frac{\partial J_{\mathrm{obj}}}{\partial \hat{a}_i}&=-\int_0^1\frac{1}{2\sqrt[3]{x_1(s)}}\frac{\partial x_1(s)}{\partial \hat{a}_i}\mathrm{d}s\\&=-\int_0^1\frac{1}{2\sqrt[3]{x_1(s)}}N_{i,p}(s)\,\mathrm{d}s.\end{aligned}\tag{26}$$

According to properties of B-splines, $N_{i,p}(s)$ is a non-zero polynomial only on $[\mathbf{s_n}(i),\mathbf{s_n}(i+p+1))$. So Eq. (26) can be reduced to

$$\frac{\partial J_{\mathrm{obj}}}{\partial \hat{a}_i}=-\int_{\mathbf{s_n}(i)}^{\mathbf{s_n}(i+p+1)}\frac{1}{2\sqrt[3]{x_1(s)}}N_{i,p}(s)\,\mathrm{d}s.\tag{27}$$

For the boundary setting $x_1(0)=0$ and $x_1(1)=0$ (i.e. zero boundary velocity for each joint), the term $\frac{1}{2\sqrt[3]{x_1(s)}}N_{i,p}(s)$ will approach to infinite for $s\to 0$ or $s\to 1$. This means that if we use uniform nodes distribution, then the parameter sensitivity would be very large for the parameters near the boundary. To deal with this ill-conditioned problem, the roots of the Chebyshev polynomial (refer to Mason and Handscomb[27]) are used as the grid nodes

$$s_i=\frac{1}{2}\left(\cos\left(\frac{2(K-i-1)-1}{2(K-1)}\pi\right)+1\right),\quad i=1,2,\ldots,K-p+1,\tag{28}$$

which are shown in Fig. 3.

4.3. The number of constraint reference points

For optimal control problem (20), the optimal constraint structure can be proven to be “bang-bang" by using the extended maximum principle. This means at least one of the process constraints is in saturation at any time. So the optimal trajectory is always charged by process constraints.

https://doi.org/10.1017/S0263574715000247 Published online by Cambridge University Press

The parameterized trajectory (23) has $K+2$ decision variables. Since $x_1(0)$ and $x_1(1)$ are known, only K decision variables need to be optimized, which are

$$\mathbf{X} = \{\hat{a}_1, \ldots \hat{a}_K\}. \tag{29}$$

We call this the *decision parameter vector*.

According to the common optimization approaches,[9,10,19,23] the continuous process torque and voltage constraints are considered only at certain finite points and assumed none of the process constraints is violated between any two adjacent points.

Since the optimal trajectory is always charged by process constraints and the process constraints are linear in the decision vector $\mathbf{X}$, the number of constraint reference points should be at least K, otherwise the optimized trajectory is not unique.

4.4. Convex program formulation and solution

As mentioned in Section 3.2, the desired optimal trajectory can be obtained by solving a convex optimal control problem (20). Then based on the B-spline trajectory parameterization in Section 4.1, the final convex optimization problem can be given as follows.

The constraint reference nodes are

$$\bar{s}_j = \begin{cases} \frac{1}{2}s_1, & j = 1, \\ \frac{1}{2}\left(s_{j-1} + s_j\right), & j = 2, \ldots, K-p+1, \\ \frac{1}{2}\left(s_{K-p+1}+1\right), & j = K-p+2. \end{cases} \tag{30}$$

In this paper, the degree of B spline is $p = 2$, so we have $K - p + 2 = K$, which means that the constraint reference nodes satisfy the number requirement mentioned in Section 4.3.

The values of each state variable $x_1,\ x_2,\ x_3$ at node $\bar{s}_j$ are as follows:

$$\begin{cases} x_1\left(\bar{s}_j\right) = \sum_{i=0}^{K+1} N_{i,p}\left(\bar{s}_j\right)\hat{a}_i \\ x_2\left(\bar{s}_j\right) = \frac{1}{2}\sum_{i=0}^{K+1} N'_{i,p}\left(\bar{s}_j\right)\hat{a}_i \\ x_3\left(\bar{s}_j\right) = \frac{1}{2}\sum_{i=0}^{K+1} N''_{i,p}\left(\bar{s}_j\right)\hat{a}_i \end{cases} \quad \text{for} \quad j = 1, 2, \ldots, K. \tag{31}$$

The objective function can be approximated as

$$J_{obj} = \int_0^1 \frac{1}{\sqrt{x_1(s)}}\mathrm{d}s \approx \sum_{j=1}^{K}\left(\frac{\Delta\bar{s}_j}{\sqrt{x_1\left(\bar{s}_j\right)}}\right), \tag{32}$$

with $\Delta\bar{s}_j = s_j - s_{j-1}$. And the robotic dynamics at node $\bar{s}_j$ can be written as

$$\begin{aligned} &\tau\left(\bar{s}_j\right) = \mathbf{m}\left(\bar{s}_j\right)x_2\left(\bar{s}_j\right) + \mathbf{c}\left(\bar{s}_j\right)x_1\left(\bar{s}_j\right) + \mathbf{g}\left(\bar{s}_j\right), \\ &\tau'\left(\bar{s}_j\right) = \mathbf{m}\left(\bar{s}_j\right)x_3\left(\bar{s}_j\right) + \left(\mathbf{m}'\left(\bar{s}_j\right) + 2\mathbf{c}\left(\bar{s}_j\right)\right)x_2\left(\bar{s}_j\right) + \mathbf{c}'\left(\bar{s}_j\right)x_1\left(\bar{s}_j\right) + \mathbf{g}'\left(\bar{s}_j\right), \\ &\tilde{\dot{\tau}}(\bar{s}_j) = \tau'\left(\bar{s}_j\right)\dot{s}_\tau\left(\bar{s}_j\right) \\ &\tilde{\mathbf{u}}\left(\bar{s}_j\right) = \left(\mathbf{L}\tau'\left(\bar{s}_j\right) + \mathbf{K}\right)\dot{s}_\tau\left(\bar{s}_j\right) + \mathbf{D}\tau\left(\bar{s}_j\right). \end{aligned}$$

Then the minimum time motion planning problem (20) can be reduced to the following convex programming problem.

$$\begin{aligned} \min_{\{\hat{a}_1,\ldots\hat{a}_K\}}\ & J_{obj} = \sum_{j=1}^{K}\left(\frac{\Delta\bar{s}_j}{\sqrt{x_1\left(\bar{s}_j\right)}}\right) \\ \text{s.t.}\quad & -\tau_{\mathrm{B}} \le \tau\left(\bar{s}_j\right) \le \tau_{\mathrm{B}}, \\ & -\dot{\tau}_B \le \tilde{\dot{\tau}}(\bar{s}_j) \le \dot{\tau}_B, \\ & -\mathbf{u}_{\mathrm{B}} \le \tilde{\mathbf{u}}\left(\bar{s}_j\right) \le \mathbf{u}_{\mathrm{B}}, \quad j = 1, 2, \ldots, K. \end{aligned} \tag{33}$$

https://doi.org/10.1017/S0263574715000247 Published online by Cambridge University Press

Table I. Model data of the test manipulator.

	$Mass$(kg)	R(m)	J_L(kgm^2)	J_T(kgm^2)	L(m)
Basic link	–	–	5.0	–	0.1
Arm 1	6.6	0.55	0.1	0.6	0.75
Arm 2	4.2	0.60	0.02	0.3	0.75

Table II. Motor dynamics parameters.

$R_i = 5$ ohm	$L_i = 0.1$ H
$K_i{}^e = 0.3$ (V.s/rad)	$K_i{}^\tau = 2$
$u_{iB} = 36$ V	$i = 1, 2, 3$

The following boundary conditions are also needed: $\hat{a}_0 = x_1(0)$, $\hat{a}_{K+1} = x_1(1)$, $\frac{1}{2}\sum_{i=0}^{K+1} N'_{i,p}(0)\hat{a}_i = x_2(0)$, $\frac{1}{2}\sum_{i=0}^{K+1} N'_{i,p}(1)\hat{a}_i = x_2(1)$, which are also linear in $\hat{a}_i$.

We are now in a position of solving problem (33). Since problem (33) is convex, any local optimum is also the globally optimal. Hence, any conventional gradient-based optimization technique such as SQP[23] can be used to solve the problem efficiently.

4.5. Interpolation points generation

Finally, it is worth to mention that, with the help of the trajectory formulation (23), the interpolation points can be computed efficiently.

Since $x_1(s) = \dot{s}^2(s)$, we can obtain the information of $a'(s)$ and $a''(s)$ easily. Suppose s_k is the last interpolation point at time t_k. Using Taylor's expansion for the parameter s, we have the following approximate formula for the next interpolation point s_{k+1}:

$$s_{k+1} = s_k + \dot{s}_k T + \frac{1}{2}\ddot{s}_k T^2 + \frac{1}{6}\dddot{s}_k T^3, \quad s_0 = 0, \quad k = 0, 1, 2, \ldots, \tag{34}$$

where T is the sampling interval of the digital controller. By Eqs. (9) and (11), we have $\dot{s}_k = \sqrt{x_1(s_k)}$, $\ddot{s}_k = x_2(s_k)$, $s^{\cdots}{}_k = x_1(s_k)x_3(s_k)$, where $x_1(s_k)$, $x_2(s_k)$, $x_3(s_k)$ can be found in Eq. (31).

5. Numerical Experiments

In this section, a series of numerical experiments are executed to verify the effectiveness of the proposed approach. The experimental manipulator is a three-DOF elbow manipulator presented in Pfeiffer and Johanni.[28] The data of the model are listed in Table I and Table II, in which the definition of each character can be found in Pfeiffer and Johanni.[28]

A double parabola in the robot work space is chosen as the predefined path.[28] In parametric form, the path is given as

$$\begin{cases} x(s) = 0.5, \\ y(s) = 20s^3 - 30s^2 + 10s, \\ z(s) = s - 0.5, \end{cases}$$

and $s \in [0, 1]$.

The MATLAB SQP routine *fmincon* is used to solve the convex optimization problem (33). All the numerical solutions are run on a laptop with Windows 32-bit system, 2.5GHz Core i3 processor, and 2GB RAM memory.

The numerical test is divided into two parts. The first part is trajectory planning test to verify the effectiveness of the numerical optimization strategy, mainly about the planning time and the quality of the results. The second part is called trajectory tracking test. By constructing a simulation environment of real robotic manipulator, we test the tracking performance of robot along the planned trajectory obtained from part 1.

https://doi.org/10.1017/S0263574715000247 Published online by Cambridge University Press

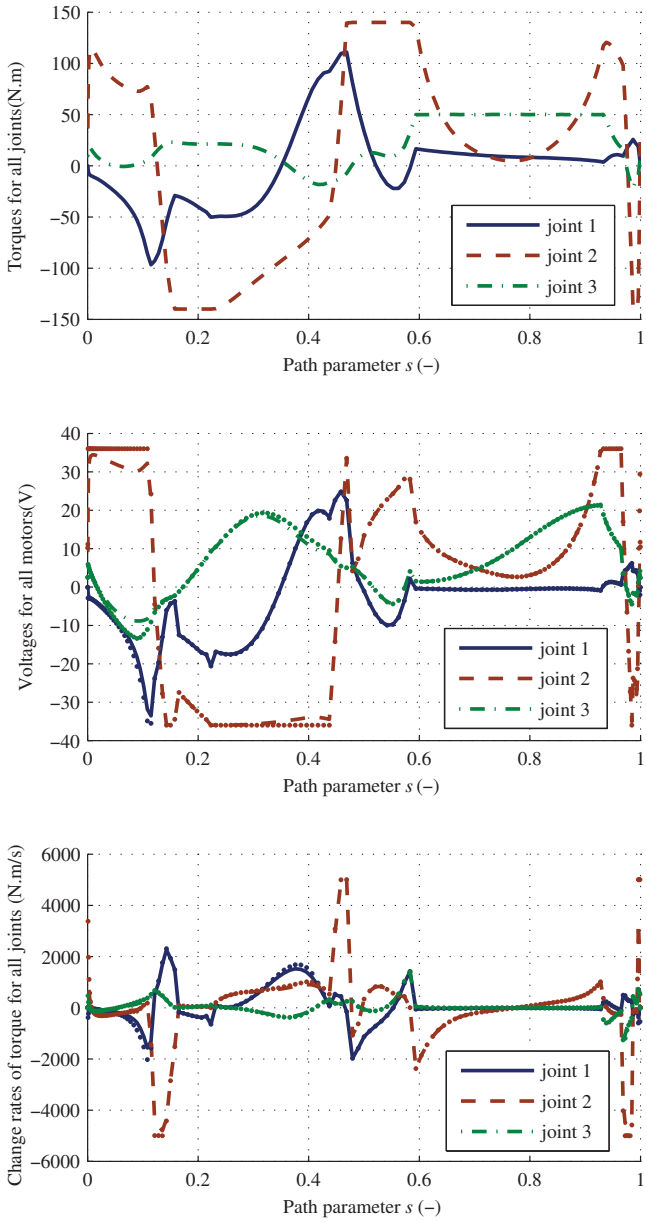


Fig 4. Optimized torques (a), voltages (b), and change rate of torque (c) of all three joints obtained using the proposed approach, while dot lines in subfigure (b) and (c) denote the virtual voltages and virtual change rates of torque, respectively.

The following parameters of DC motors are applied in our tests: The motor voltage bounds are 36V for both the trajectory planning and trajectory tracking tests, while the joint torque bounds are [140; 140; 50] N.m and the bounds of the change rates of the torque are [5000; 5000; 5000] N.m/s. We can check that the constraint settings satisfy the assumption in Eq. (21). By Theorem 2, the minimum time trajectory obtained by the proposed approach is also feasible for the original problem.

For convenience, we use T-MTM, VV+T-MTM, and RV+T-MTM to denote problem (17) with only torque constraints, problem (20) with virtual voltages and virtual torque change rates constraints, and problem (16) with real voltages and torque change rates constraints, respectively.

5.1. Trajectory planning performance

By solving the convex optimization problem (33) for this example, the optimal torques and voltages are obtained and shown in Fig. 4. The singularity problem of numerical optimization reported by

https://doi.org/10.1017/S0263574715000247 Published online by Cambridge University Press

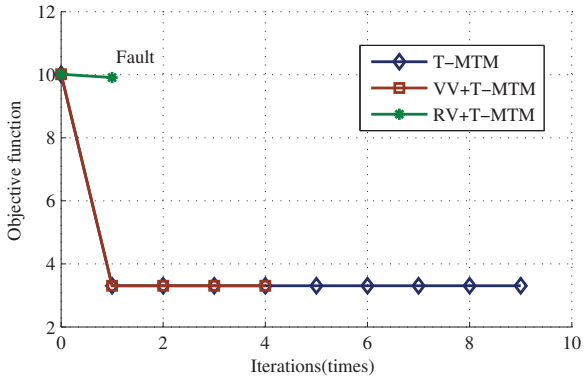


Fig 5. Convergence performances of using direct transcription algorithm to compute trajectories of T-MTM, VV+T-MTM, RV+T-MTM .

Verscheure *et al.*,[10] Shiller,[1] and Chen and Desrochers[14] is solved by adding a small amount of regularization into the objective function to penalize torque jumps as used in Verscheure *et al.*[10]

Fig. 4 shows that the optimized torque, change rate of the torque, and (virtual) voltage have "bang-bang" structures as expected. The controlling constraints for the motion are respectively as follows: the virtual voltage of joint 2 in [0, 0.15], change rate of the torque of joint 2 in [0.15, 0.17], torque of joint 2 in [0.17, 0.22], change rate of the torque of joint 2 in [0.22, 0.42], torque of joint 2 in [0.42, 0.59], torque of joint 1 in [0.59, 0.95], voltage of joint 2 in [0.95, 0.97], change rate of the torque of joint 2 in [0.97, 0.1]. The bang-bang structure is a good indicator for the numerical solution to be the optimal solution.

In Fig. 4(b), the dot lines represent the virtual voltages and the solid lines represent the real voltages. First, we can see from Fig. 4(b) that the virtual voltage is a very tight approximation to the real voltage. Second, when the virtual voltage approaches to saturation, the corresponding real voltage could remain feasible and this is consistent with the analysis given in Section 3.2. In our example, this happens clearly for joint 2 in the interval [0.05, 0.15]. From Fig. 4(c), similar facts can be observed for the virtual change rate of the torque. Above all, since the objective function of the studied optimal control problems (16) and (20) is minimum time, we can say that the VV+T-MTM trajectory obtained is time optimal for problem (20) and is near time optimal for problem (16).

Figure 5 shows the convergence rate of the direct transcription algorithm for computing the T-MTM, VV+T-MTM, and RV+T-MTM trajectories. From Fig. 5, we can see that the optimal solutions for T-MTM and VV+T-MTM can be achieved by 2 or 3 iterations only. For the RV+T-MTM problem and the same initial value, the direct transcription algorithm is not convergence because of the non-convexity of the problem.

The motion times for the T-MTM, VV+T-MTM, and RV+T-MTM trajectories are 1.617 s, 1.794 s, and 1.7435 s, respectively. This shows that VV+T-MTM gives very nice approximation to RV+T-MTM. The solution times of T-MTM and VV+T-MTM are respectively 0.76 s and 2.26 s. For comparison purposes, the solution time of RV+T-MTM is also given. For an arbitrary initial value, the solution procedure for RV+T-MTM is generally not convergent, since the problem is non-convex and the initial value is usually far away from the optimal ones. The computation times for solving RV+T-MTM are respectively 10.9 s and 11.8 s when using the solutions of T-MTM and VV+T-MTM as initial values.

Figure 6 plots the parameter velocity trajectories for the T-MTM, VV+T-MTM, RV+T-MTM, and the *velocity limit curve* (VLC) introduced in Shiller,[1] which gives an upper bound for the parameter velocity. It can be seen that the results for VV+T-MTM and RV+T-MTM are very close, except in the interval [0.05, 0.15]. The optimized velocity, torque, voltage, and change rate of the torque for each joint are presented in Figs. 7–9, respectively. From Figs. 6–9, we can see that the trajectory of VV+T-MTM is very close to the trajectory of RV+T-MTM. From Figs. 7–9, we see that by adding the motor dynamics constraints, the torque functions become smoother than that of T-MTM, which will lead to smaller tracking errors as shown in the next section.

https://doi.org/10.1017/S0263574715000247 Published online by Cambridge University Press

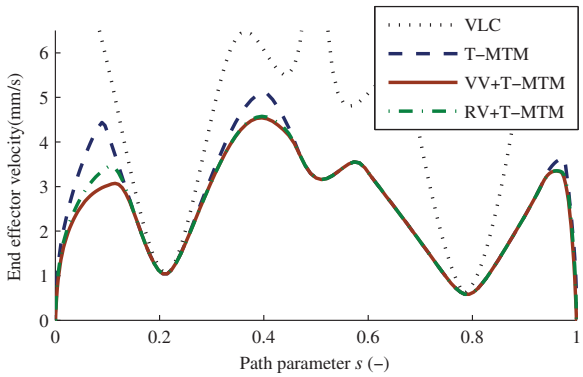


Fig 6. VLC and parameter velocity trajectories for the T-MTM, VV+T-MTM, and RV+T-MTM.

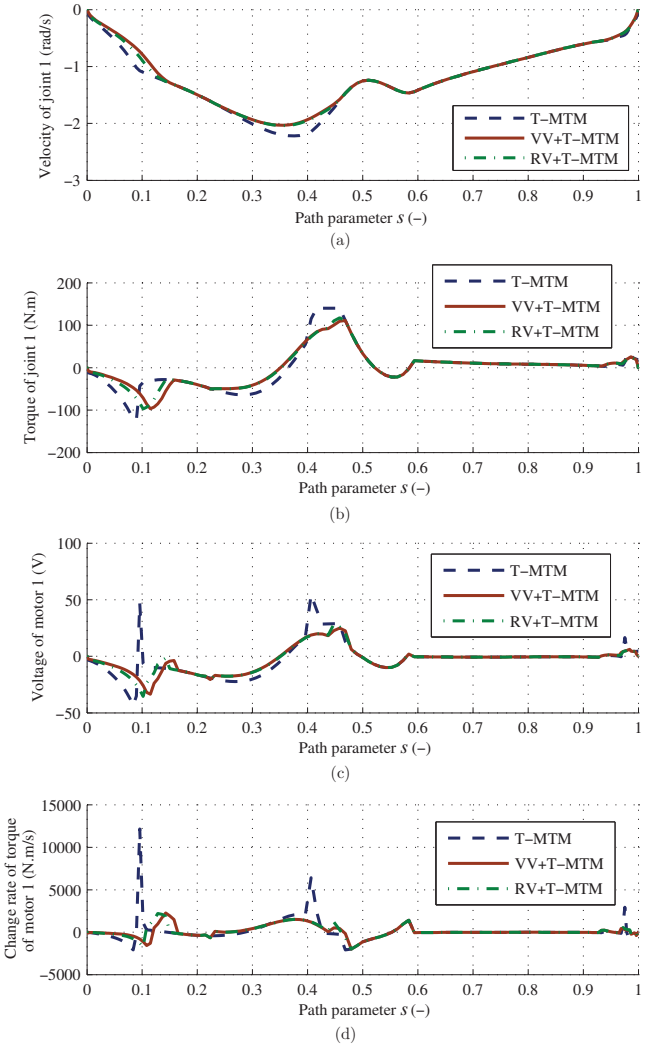


Fig 7. Optimized velocity(a), torque (b), voltage(c), and change rate of torque (d) of joint 1 for T-MTM, VV+T-MTM, and RV+T-MTM, respectively.

5.2. Trajectory tracking performance

To check the tracking performance of the trajectories obtained in the preceding section, we use the control model in Fig. 10, which has the same dynamics and DC motor dynamics described in this paper. Also, a PD controller with voltage feedforward is used to control each joint and control voltage saturation is also considered. The purpose of using the simple and less powerful PD controller is that

https://doi.org/10.1017/S0263574715000247 Published online by Cambridge University Press

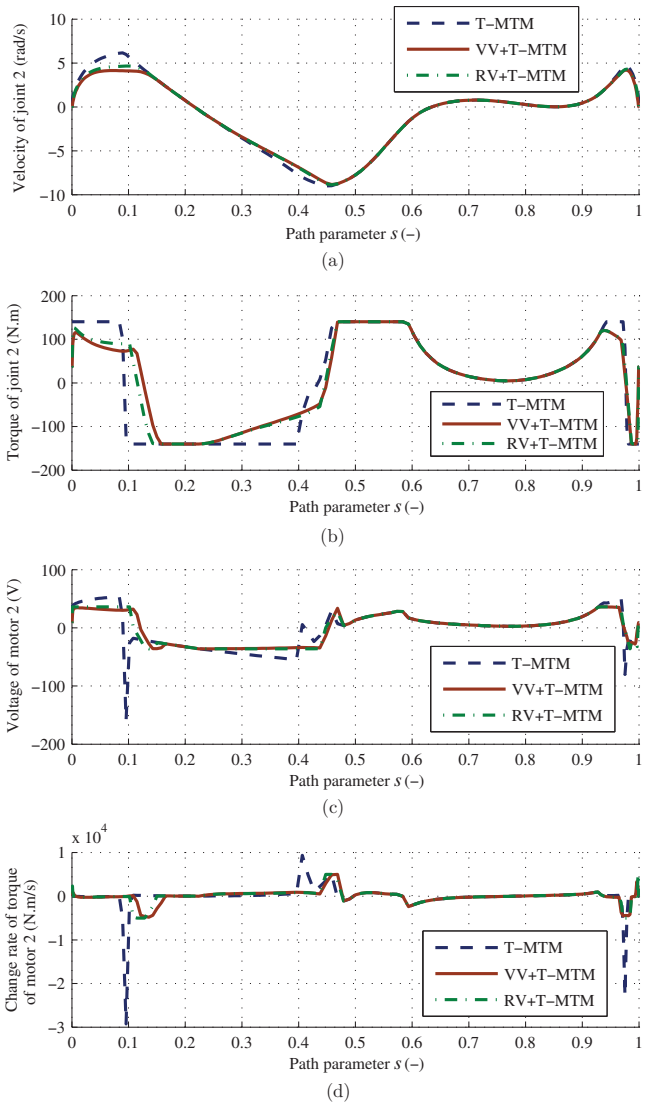


Fig 8. Optimized velocity(a), torque (b), voltage(c), and change rate of torque (d) of joint 2 for T-MTM, VV+T-MTM, and RV+T-MTM, respectively.

if the generated trajectory performs good for the PD controller, then it is expected that the trajectory will also be practical for more advanced and powerful controllers such as PID controllers.

We build a simulation model for the robotic manipulator in Fig. 10 in MATLAB's Simulink environment and use this model to check the tracking performance. Although differences between the real and the virtual tests actually exist, MATLAB's Simulink is widely recognized to be a mature product which can give valid test results for the key behavior of the real dynamic system and the qualitative conclusions thus obtained should be consistent with the real performance of the robot system.

Using the interpolation algorithm from Section 4.5, the optimized spline trajectories are resampled as sequences of reference points for each joint position within each sampling interval T of the digital controller and fed into the MATLAB simulator to obtain the tracking performance.

The tracking performance for the T-MTM, VV+T-MTM, and RV+T-MTM trajectories are plotted in Figs. 11–13, respectively. As seen in Fig. 11(c), due to voltage saturation of joint 2, the motor cannot export enough torque to force the joint position on the reference trajectory when the change rate of the torque are too high for the T-MTM trajectory. As a result, large tracking errors occur, with the maximum tracking error approaching to 0.7 rad for the T-MMM trajectory. From Figs. 12 and 13, we can see that by adding the voltage limits, the maximum tracking error is reduced below

https://doi.org/10.1017/S0263574715000247 Published online by Cambridge University Press

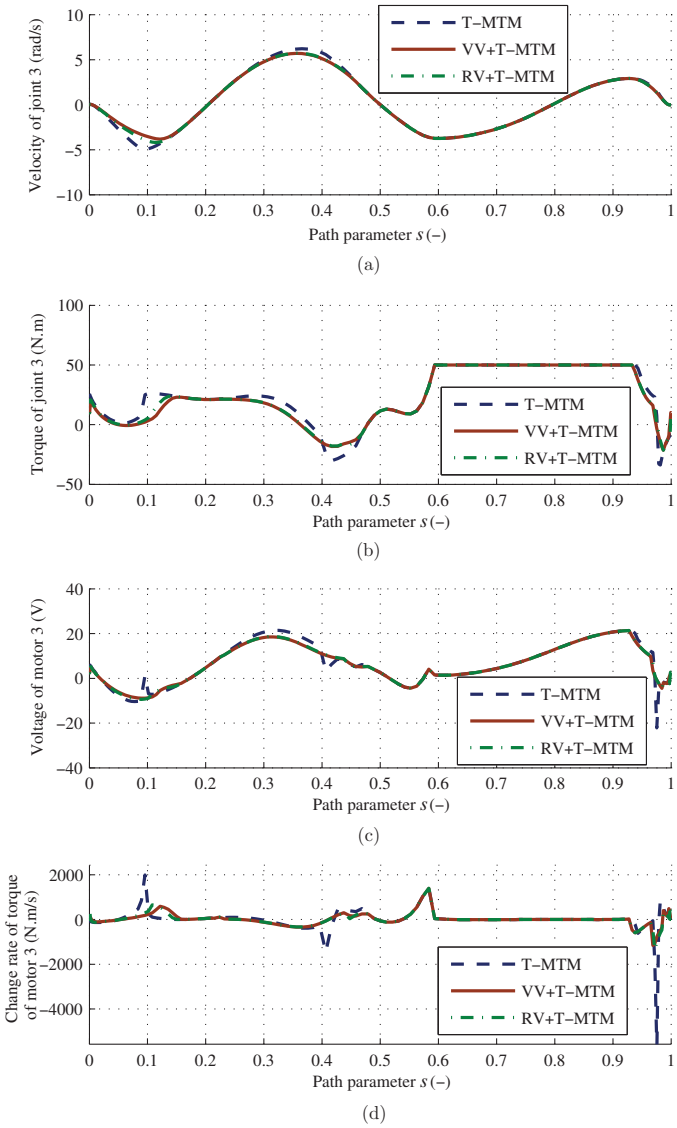


Fig 9. Optimized velocity(a), torque (b), voltage(c), and change rate of torque (d) of joint 3 for T-MTM, VV+T-MTM, and RV+T-MTM, respectively.

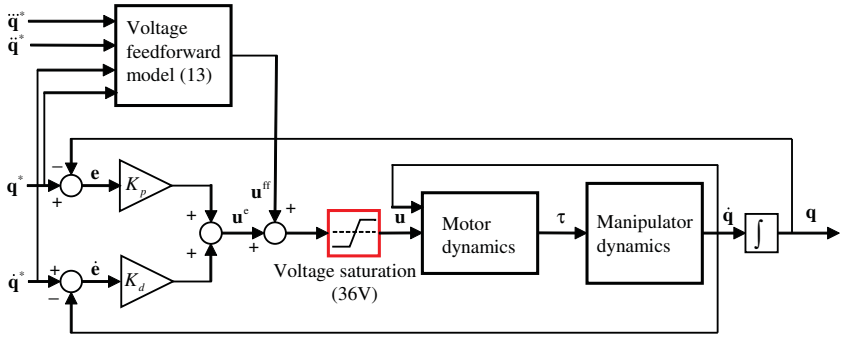


Fig 10. The experimental setup.

https://doi.org/10.1017/S0263574715000247 Published online by Cambridge University Press

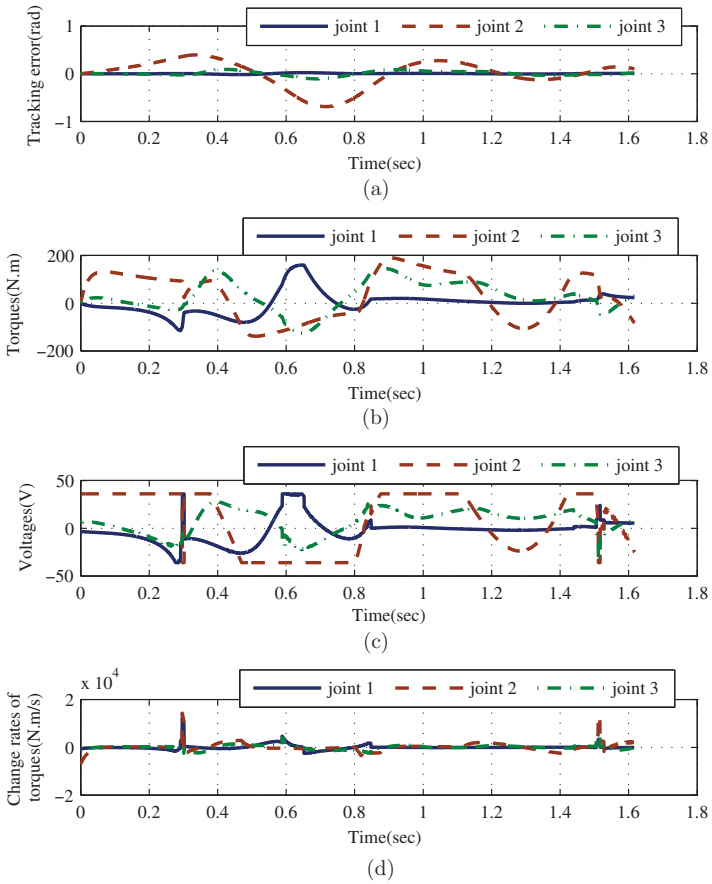


Fig 11. Tracking performance of the T-MTM trajectory: (a) tracking error of each joint, (b) executed torque of each joint, (c) executed voltage of each joint, (d) change rate of each joint torque.

0.02 rad for the VV+T-MTM and RV+T-MTM trajectories. Furthermore, the moving time for the VV+T-MTM and RV+T-MTM trajectories are 1.79 s and 1.74 s, respectively, which are about 11% and 7% losses comparing to the moving time of 1.67 s for the T-MTM trajectory. In summary, the maximum tracking error can be reduced up to 97% with a moving time loss below 10%, which shows the effectiveness of introducing the bounds of voltages and change rates for the torque.

5.3. More experimental results

In this subsection, a more detailed experiment is conducted. Five sets of joint torque bounds, as shown in Table III, are applied to plan different trajectories in this experiment, while the voltage bounds of drive motors and the change rate of the torque bounds remain unchanged. The trajectory planning test as in Subsection 5.1 and the trajectory tracking test as in Subsection 5.2 are implemented for each of the five torque bounds. The experimental results are listed in Table IV, where the thermal dissipation is calculated by

$$CQ = \int_0^{t_f} \sum_{i=1}^{n} Q_i \mathrm{d}t = \int_0^{t_f} \left(\sum_{i=1}^{n} I_i^2 R_i \right) \mathrm{d}t,$$

and is used to denote the energy loss of the motor.

Below are the main observations from Table IV.

To realize the RV+T-MTM solution, the optimum solutions of T-MTM and VV+T-MTM are used as the initial values. The results indicate that the computation times are similar for these two initial values and in the solution processes we also observe that the optimum solutions with the two different initial values are the same. It is also clear that the solution time for RV+T-MTM is significantly larger than that of VV+T-MTM.

https://doi.org/10.1017/S0263574715000247 Published online by Cambridge University Press

Table III. Five levels of torque bounds setting.

	Torque boundary setting [joint1; joint2; joint3](N.m)
1	[140; 140; 50]
2	[126; 126; 45]
3	[112; 112; 40]
4	[98; 98; 35]
5	[84; 84; 30]

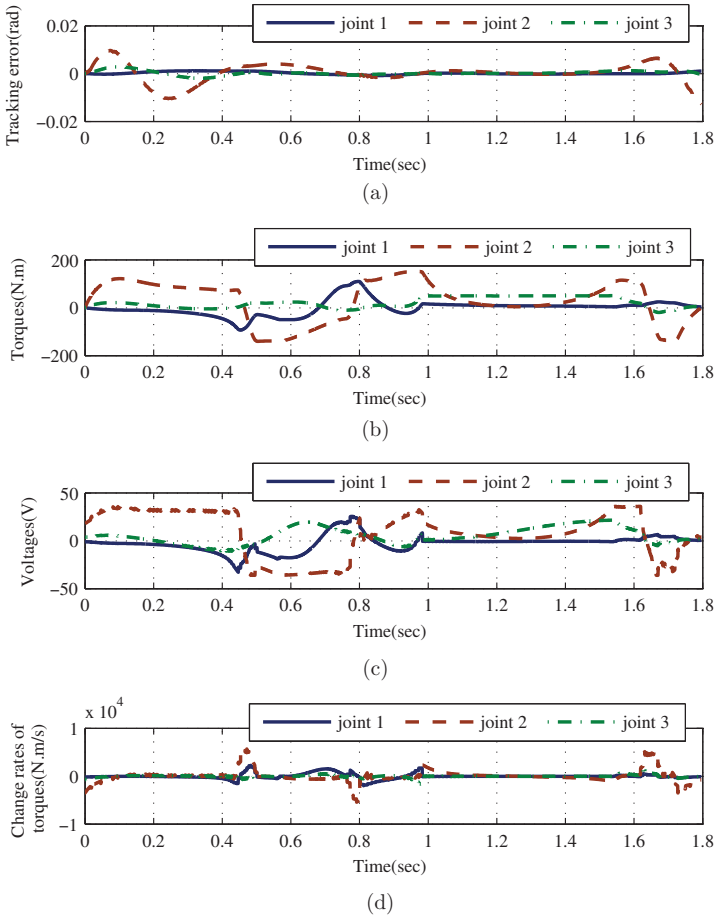


Fig 12. Tracking performance of the VV+T-MTM trajectory: (a) tracking error of each joint, (b) executed torque of each joint, (c) executed voltage of each joint, (d) change rate of each joint torque.

Second, for small torque bounds(such as Test 4 and 5), the tracking performances of the three cases (T-MTM, VV+T-MTM and RV+T-MTM) are similar, and for larger torque bounds(such as Test 1, 2 and 3), the advantage of adding dynamics constraints becomes apparent: in Test 1, the maximum tracking error of VV+T-MTM is reduced to 1.8% of that of T-MTM with the cost of 11% more motion time. A more intuitive chart is plotted in Fig. 14 to present the performance differences among T-MTM, VV+T-MTM, RV+T-MTM. In Fig. 14, the machining precision is characterized by maximum tracking error of all three joints. From Fig. 14(a), we can see that for T-MTM, for high speed motion, the tracking error becomes significant, while for VV+T-MTM and RV+T-MTM, the tracking error is stable for all reasonable motion times. So it is necessary to consider motor dynamics for high accuracy and high speed motions. Figure 14(b) shows the proposed VV+T-MTM has lower energy loss than T-MTM.

Third, VV+T-MTM and RV+T-MTM perform almost the same in all cases, which shows that the virtual voltage and change rate of the torque give tight approximation to the real ones. On average, the

https://doi.org/10.1017/S0263574715000247 Published online by Cambridge University Press

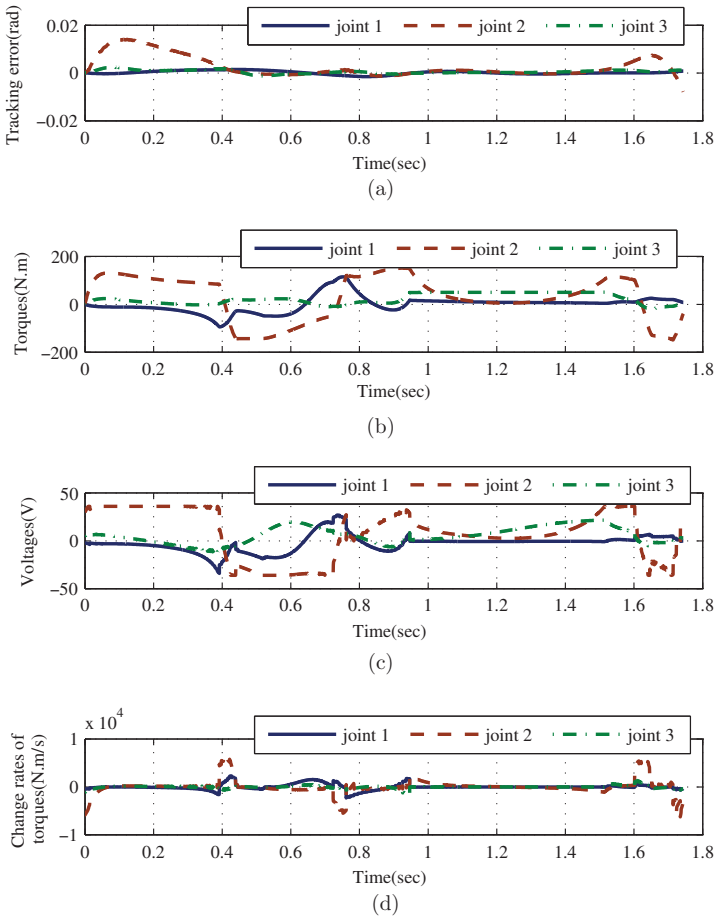


Fig 13. Tracking performance of the RV+T-MTM trajectory: (a) tracking error of each joint, (b) executed torque of each joint, (c) executed voltage of each joint, (d) change rate of each joint torque.

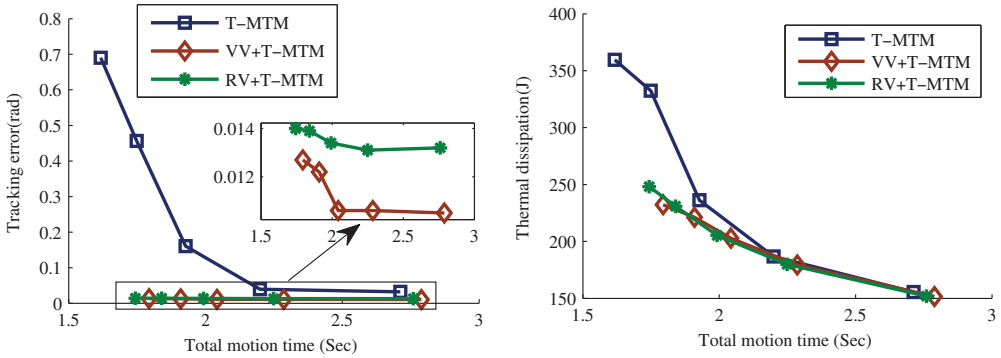


Fig 14. Motion performance comparison among T-MTM, VV+T-MTM, and RV+T-MTM trajectories.

motion time of VV+T-MTM is only 2.3% more than that of RV+T-MTM and the maxima tracking error of VV+T-MTM is 83% of that of RV+T-MTM. On the other hand, in terms of computation time, VV+T-MTM is efficiently solvable and RV+T-MTM is generally unsolvable, which shows the significant improvements of using VV+T-MTM instead of the original problem RV+T-MTM.

In summary, we have observed that introducing dynamics constraints in minimum time trajectory can significantly improve the motion precision of the robots without costing much in motion time, especially in the case of high speed motion, and using virtual voltage and virtual change rate of the torque can turn the numerically unsolvable problem into an efficiently solvable one and the results are tight approximation to the real ones.

https://doi.org/10.1017/S0263574715000247 Published online by Cambridge University Press

Table IV. Results of trajectory planning and tracking tests for the T-MTM, VV+T-MTM, RV+T-MTM along the given double parabola path.

Test	Trajectory	Planning time(s)[a]	Motion time(s)	Maximum tracking error (rad)	Mean tracking error (rad)		
					Joint 1	Joint 2	Joint 3
1	T-MTM	0.76	1.6170	0.6900	0.0060	0.2193	0.0370
	VV+T-MTM	0.76 + 1.5	1.7940	0.0127	0.0004	0.0028	0.0007
	RV+T-MTM[b]	Fault/10.9[c]/11.8[d]	1.7435	0.0140	0.0006	0.0030	0.0007
2	T-MTM	0.69	1.7485	0.4564	0.0037	0.1320	0.0237
	VV+T-MTM	0.69 + 1.49	1.9095	0.0122	0.0004	0.0027	0.0006
	RV+T-MTM[b]	Fault/15.6[c]/17.1[d]	1.8400	0.0139	0.0005	0.0028	0.0007
3	T-MTM	0.72	1.9275	0.1604	0.0012	0.0416	0.0075
	VV+T-MTM	0.72 + 1.56	2.0425	0.0106	0.0004	0.0025	0.0006
	RV+T-MTM[b]	Fault/13.3[c]/12.9[d]	1.9925	0.0134	0.0004	0.0027	0.0007
4	T-MTM	0.68	2.1990	0.0394	0.0009	0.0053	0.0014
	VV+T-MTM	0.68 + 1.59	2.2865	0.0106	0.0003	0.0021	0.0005
	RV+T-MTM[b]	Fault/10.5[c]/11.1[d]	2.2490	0.0131	0.0004	0.0023	0.0006
5	T-MTM	0.72	2.7125	0.0321	0.0006	0.0031	0.0010
	VV+T-MTM	0.72 + 1.34	2.7890	0.0105	0.0003	0.0016	0.0004
	RV+T-MTM[b]	Fault/8.1[c]/5.8[d]	2.7595	0.0132	0.0003	0.0017	0.0005

[a]The planning times are obtained when the number of the parameterized grids is 150 and the default initial value of decision vector $\mathbf{X}_0$ is 0.01. The planning times for T-MTM are obtained with the method given in ref. [24].
[b]The RV+T-MTM trajectories cannot be obtained by using the default initial values $\mathbf{X}_0$. The times reported here are those needed to solve RV+T-MTM by using the optimum solutions of T-MTM and VV+T-MTM as the initial values, respectively.
[c]By using the optimum solution of T-MTM as initial value, the planning time is the sum of the times of planning T-MTM and RV+T-MTM.
[d]By using the optimum solution of VV+T-MTM as initial value, the planning time is the sum of the times of planning T-MTM, VV+T-MTM, and RV+T-MTM.

Table V. Comparison of trajectory planning methods.

Methods	Trajectory order	Time optimal	CRT considered	Dynamics considered	Algorithm
[10]	2	Yes	No	No	CP
[16]	2	Yes	No	No	LP
[20]	3	Near optimal	Yes	No	2-steps CP
[18]	3	Yes	No	$\mathbf{L}\dot{\tau} + \mathbf{D}\tau + \mathbf{K_c}\dot{\mathbf{q}} = \mathbf{u}$	Phase plane
[19]	2	Near optimal	No	$\mathbf{D}\tau + \mathbf{K_c}\dot{\mathbf{q}} = \mathbf{u}$	CP
[21]	2	Yes	No	$\mathbf{D}\tau + \mathbf{K_c}\dot{\mathbf{q}} = \mathbf{u}$	SCP
This paper	3	Near optimal	Yes	$\mathbf{L}\dot{\tau} + \mathbf{D}\tau + \mathbf{K_c}\dot{\mathbf{q}} = \mathbf{u}$	2-steps CP

5.4. Discussion

Minimum time trajectory planning was a basic problem in robotic research and several efficient numerical methods have been proposed since 1980s.[10,16,18–21] In this section, we compare the performance of our method with the methods which deal with similar constraints, as shown in Table V.

In Table V, the trajectory order denotes the continuity of the velocity, where order 2 means a continuous velocity and order 3 means a smooth velocity. It is known that smoother velocities

https://doi.org/10.1017/S0263574715000247 Published online by Cambridge University Press

Table VI. Performance comparison of the typical trajectories.

Methods	Planning time(s)	Motion time(s)	Time loss	Max tracking error(rad)	Error reduction
[10]	0.76	1.6170	0%	0.6900	0%
[16]	0.54	1.6165	0%	0.6897	0%
[20]	1.98	1.6305	0.8%	0.6030	12.6%
[19]	1.35	1.6550	2.4%	0.1838	73%
[21]	3.41	1.7130	5.9%	0.0365	94.7%
This paper	2.26	1.7940	10.9%	0.0127	98.2%

generally lead to smaller tracking errors. CRT means the change rate of the torque. LP, CP, and SCP represent linear program, convex optimization, and sequential convex optimization, respectively. Our method uses the most general dynamic model. In Tarkiainen and Shiller,[18] although the same dynamic model is used, the manipulator gravity is neglected, and the phase plane method presented in ref. [18] can only solves very simple problems practically. The dynamic model considered in refs. [19] and [20] are simpler than ours. Also, the methods proposed in refs. [19] and [21] are not applicable to the problem in this paper. In summary, we consider the most general dynamics model and our method is also the most general one.

In Table VI, the performances of these methods are compared. The method in ref. [18] is not considered, since only very simple problems can be solved with this way. Data in Table VI are obtained based on the same trajectory parameterization and same CP solver (SQP routine in MATLAB). The torque bounds are [140;140;50] N.m in all methods. The bounds of the change rate of the torque are 5000 N.m/s. The voltage bounds are 36 V.

All methods except the second one use convex optimizations, and their running times are comparable as expected. The method in ref. [21] uses convex optimization for several times and thus runs a little bit slower than the method in this paper, which uses two convex optimizations. From refs. [10] and [20], we can see that adding the change rate of the torque as a constraint will reduce the tracking error for about 10%. From refs. [10] and [21], the results for the method in this paper, we can see that adding the voltage as a constraint will reduce the tracking error for about 90%. From ref. [21] and the results for the method in this paper, we can see that by using a more complete dynamic model, the tracking error is about 35% of that of ref. [21], while the motion time is only about 5% more than that of ref. [21]. In summary, by considering more complete dynamic constraints, the proposed method can achieve the highest machining accuracy with negligible motion time losses.

6. Conclusions

In this paper, the minimum time motion planning problem of robotic manipulators under motor dynamics constraints of each joint is considered. The change rate of the torque and the voltage of the DC motor are used to represent the complete robot dynamics. Experimental results show that adding motor dynamics constraints can significantly improve the motion precision of the robots without costing much in motion time, especially in the case of high speed motion.

Unfortunately, the minimum time motion planning of robotic manipulators under confined change rate of the torque and DC motor voltage is a nonlinear and non-convex optimization problem which is very difficult to solve numerically. As demonstrated by the experimental results, even for the powerful algorithm SQP, the problem is difficult to solve for modest sized discretization, say $K = 150$. To solve this problem, the concepts of virtual change rate of the torque and the virtual voltage are introduced, which are linear functions in the state and control variables and are very tight approximation to the real change rate of the torque and the voltage. As a result, the minimum time trajectory under robot rigid dynamics and motor dynamics is obtained by solving a convex optimization problem efficiently. Experimental results verify that the minimum time trajectory optimized by the proposed approach is close to the real optimal trajectory. Therefore, the problem proposed by Verscheure *et al.*[10] to extend their efficient approach based on convex optimization to include the change rate of the torque as a new constraint is satisfactorily solved.

https://doi.org/10.1017/S0263574715000247 Published online by Cambridge University Press

Acknowledgment
This work is partially supported by a National Key Basic Research Project of China (2011CB302400) and by a grant from NSFC (60821002).

References

1. Z. Shiller, "On singular time-optimal control along specified paths," *IEEE Trans. Robot. Autom.* **10**(4), 561–566 (1994).
2. S. D. Timar and R. T. Farouki, "Time-optimal traversal of curved paths by Cartesian CNC machines under both constant and speed-dependent axis acceleration bounds," *Robot. Cim. Int. Manuf.* **23**(5), 563–579 (2007).
3. J. Y. Dong, P. M. Ferreira and J. A. Stori, "Feedrate optimization with jerk constraints for generating minimum-time trajectories," *Int. J. Mach. Tools Manu.* **47**(12–13), 1941–1955 (2007).
4. A. Gasparetto and V. Zanotto, "A technique for time-jerk optimal planning of robot trajectories," *Robot. Cim. Int. Manuf.* **24**, 415–426 (2008).
5. B. Sencer, Y. Altintas and E. Croft, "Feed optimization for five-axis CNC machine tools with drive constraints," *Int. J. Mach. Tools Manu.* **48**, 733–745 (2008).
6. T. Kröger and F. M. Wahl, "Online trajectory generation: Basic concepts for instantaneous reactions to unforeseen events," *IEEE Trans. Robot.* **26**(1), 94–111 (2010).
7. K. Zhang, X. S. Gao, H. B. Li and C. M. Yuan, "A greedy algorithm for feed-rate planning of CNC machines along curved tool paths with confined jerk for each axis," *Robot. Cim. Int. Manuf.* **28**, 47–483 (2012).
8. J. E. Bobrow, S. Dubowsky and J. S. Gibson, "Time-optimal control of robotic manipulators along specified paths," *Int. J. Robot. Res.* **4**(3), 3–17 (1985).
9. D. Constantinescu and E. A. Croft, "Smooth and time optimal trajectory planning for industrial manipulators along specified paths," *J. Robot. Syst.* **17**(5), 233–249 (2002).
10. D. Verscheure, B. Demeulenaere, J. Swevers, J. De Schutter and M. Diehl, "Time-optimal path tracking for robots: a convex optimization approach," *IEEE Trans. Autom. Control* **54**(10), 2318–2327 (2009).
11. M. H. Korayem, M. Irani, A. Charesaz, A. H. Korayem and A. Hashemi, "Trajectory planning of mobile manipulators using dynamic programming approach," *Robotica* **31**(4), 643–656 (2013).
12. A. Trevisani, "Planning of dynamically feasible trajectories for translational, planar, and unconstrained cable-driven robots," *J. Syst. Sci. Complex.* **26**(5), 695–717 (2013).
13. M. J. Sadigh and S. Mansouri. "Application of phase-plane method in generating minimum time solution for stable walking of biped robot with specified pattern of motion," *Robotica* **31**(6), 837–851 (2013).
14. Y. B. Chen and A. A. Desrochers, "A proof of the structure of the minimum-time control law of robotic manipulators using a Hamiltonian formulation," *IEEE Trans. Robotic Autom.* **6**(3), 388–393 (1990).
15. P. Reynoso-Mora, W. Chen and M. Tomizuka, "On the time-optimal trajectory planning and control of robotic manipulators along predefined paths," *Proceedings of the 2013 American Control Conference* Washington DC, USA (2013) pp. 371–377.
16. Q. Zhang, J. X. Guo, X. S. Gao and S. Li, "Tractable algorithm for robust time-optimal trajectory planning of robotic manipulators under confined torque," *Int. J. Comput. Commun. Control* **10**(1), 123–135 (2015).
17. T. J. Tarn, A. K. Bejczy, X. Yun and Z. Li, "Effect of motor dynamics on nonlinear feed-back robot arm control," *IEEE Trans. Robot. Autom.* **7**, 114–122 (1991).
18. M. Tarkiainen and Z. Shiller, "Time Optimal Motions of Manipulators with Actuator Dynamics," *IEEE International Conference on Robotics and Automation* Atlanta (1993).
19. T. Ardeshiri, M. Norrlof, J. Lofberg and A. Hansson, "Convex Optimization Approach for Time-Optimal Path Tracking of Robots with Speed Dependent Constraints," *18th IFAC World Congress* Milano, Italy (2011).
20. Q. Zhang, S. Li and X. S. Gao, "Practical Smooth Minimum Time Trajectory Planning for Path Following Robotic Manipulators," *Proceedings of The 2013 American Control Conference*, Washington DC (2013) pp. 2784–2789.
21. F. Debrouwere, W. Van Loock, G. Pipeleers, Q. T. Dinh, M. Diehl, J. De Schutter and J. Swevers, Time-optimal path following for robots with convex-concave constraints using sequential convex programming. *IEEE Trans. Robot.* **29**(6) (2013).
22. C. S. Chiu, K. Y. Lian and T. C. Wu, "Robust adaptive motion/force tracking control design for uncertain constrained robot manipulators," *Automatica* **40**, 2111–2119 (2004).
23. C. Buskens and H. Maurer, "SQP-methods for solving optimal control problems with control and state constraints: adjoint variables, sensitivity analysis, and real time control," *J. Comput. Appl. Math.* **120**, 85–108 (2000).
24. W. Fan, X. S. Gao, C. H. Lee, K. Zhang and Q. Zhang. "Time-optimal interpolation for five-axis CNC machining along parametric tool path based on linear programming," *Int. J. Adv. Manuf. Technol.* **69**(5), 1373–1388 (2013).
25. K. Zhang, C. M. Yuan and X. S. Gao, "Efficient algorithm for feedrate planning and smoothing with confined chord error and acceleration for each axis," *Int. J. Adv. Manuf. Technol.* **66**(9), 1685–1697 (2013).
26. C. Yuan, K. Zhang and W. Fan, "Time-optimal interpolation for CNC machining along curved tool pathes with confined chord error," *J. Syst. Sci. Complex.* **26**(5), 836–870 (2013).

https://doi.org/10.1017/S0263574715000247 Published online by Cambridge University Press

27. J. C. Mason and D. C. Handscomb, Chebyshev Polynomials (CRC Press, 2002). Boca Raton, Florida, USA.
28. F. Pfeiffer and R. Johanni, "A concept for manipulator trajectory planning," *IEEE J. Robot. Autom.* **3**(2), 115–123 (1987).
29. N. M. Patrikalakis and T. Maekawa, *Shape Interrogation for Computer Aided Design and Manufacturing* (Springer Berlin Heidelberg, Germany, 2002).

https://doi.org/10.1017/S0263574715000247 Published online by Cambridge University Press